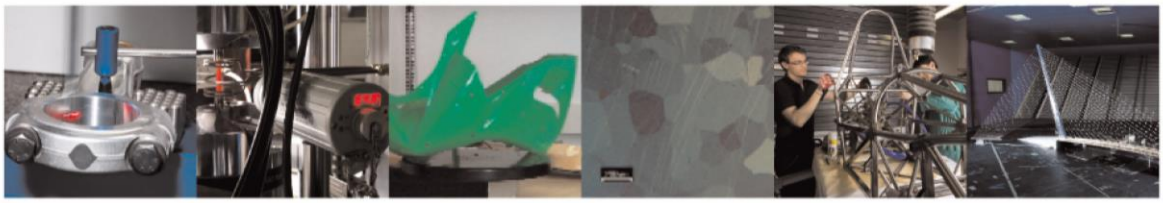

Calibration and Validation of a Mechanistic Micromilling Force Prediction Model

Annoni, Massimiliano; Pusterla, Nicola; Rebaioli, Lara; Semeraro, Quirico

Calibration and validation of a mechanistic micromilling force prediction model

Massimiliano Annoni, first author[1]
Politecnico di Milano
Via G. La Masa, 1
20156 Milano, ITALY
e-mail: massimiliano.annoni@polimi.it

Nicola Pusterla, second author
Politecnico di Milano
Via G. La Masa, 1
20156 Milano, ITALY

Lara Rebaioli, third author
Politecnico di Milano
Via G. La Masa, 1
20156 Milano, ITALY
e-mail: lara.rebaioli@polimi.it

Quirico Semeraro, fourth author
Politecnico di Milano
Via G. La Masa, 1
20156 Milano, ITALY
e-mail: quirico.semeraro@polimi.it

Abstract

Mechanistic force prediction models require a calibration phase to determine the cutting coefficients describing the tool-target material interaction. The model prediction performance depends on the experimental correctness and representativeness of input data, especially in micromilling, where facing process uncertainties is a big challenge. The present paper focuses on input data correctness introducing a clear and repeatable calibration experimental procedure based on accurate force data acquisitions. Input data representativeness has been directly connected to the calibration window choice, i.e. the selection of the space of process

[1]Corresponding author at: POLITECNICO DI MILANO - Dipartimento di Meccanica - Sezione Tecnologie Meccaniche e Produzione, Via G. La Masa, 1 - Milano - Italy. Area code: 20156. Ph.: +39 02 23998530 (Secretary); +39 02 23998536 (Direct). Fax: +39 02 23998585
E-mail: massimiliano.annoni@polimi.it

parameters combinations used to calibrate the model. Also the model validation has to be carefully carried out to make the model significant: the present paper proposes a clear and repeatable validation procedure based on the model performance index calculation over the whole process operating window, i.e. the space of parameters where the process works correctly. An objective indication of the model suitability can be obtained by applying this procedure. Comparisons among prediction performances produced by different calibration windows are allowed. This paper demonstrates how the calibration window selection determines the model prediction performance, which seems to improve if calibration is carried out where forces assume high values. Some important considerations on the process parameters role on cutting forces and on the model capability have also been drawn from the model validation results.

Keywords: micromilling, force model, force acquisition, model calibration, model validation

Nomenclature

A_i	parameters of the normal cutting force coefficient function
a_e	width of cut
a_p	depth of cut
B_i	parameters of the frictional cutting force coefficient function
C_i	parameters of the chip flow angle function
D	mill diameter
F_f	frictional cutting force
F_n	normal cutting force
FRF	frequency response function
f_s	force sampling frequency
F_x, F_y, F_z	cutting force components along the machine tool axes
f_z	feed per tooth
I	number of flutes
j	acquired force point index
K_f	frictional cutting force coefficient
K_n	normal cutting force coefficient
n	spindle rotational speed
N	total amount of acquired force points
R	resultant cutting force
$RMSE$	root mean square error
r_e	cutting edge radius
t_c	uncut chip thickness
v_c	cutting speed
X, Y, Z	machine tool axes
$\alpha_{r,e}$	partial effective rake angle
$\alpha_{r,n}$	nominal rake angle
ϕ	disk element angular position
$\Delta\theta_s$	sampled force angular pitch
θ	cutting edge angular position
θ_c	chip flow angle
θ_h	helix angle
Subscripts	
i	machine tool axis index
j	acquired force point index
meas	measured
pred	predicted
complete	“complete” calibration window
reference	“reference” calibration window

1 Introduction

Micromilling force prediction models are the core of process planning since they are the link between process parameters and the required workpiece characteristics, i.e. the final result of

the working operation. The force prediction model by itself is a tool to evaluate the feasibility of the operation in terms of allowed force, torque and power, but also to predict the final workpiece quality without implying the use of experimental resources.

In fact cutting forces can be considered an indirect workpiece quality index in micromilling, since they are responsible for both the tool and the thin workpiece features deformations, i.e. for the final manufacturing errors. Predicting forces in the process planning phase is a powerful capability to achieve the required quality on the workpiece. Moreover, forces are measureable on-line, allowing an effective process monitoring.

This paper deals with the calibration and validation of a mechanistic micromilling cutting force prediction model. After reviewing the different types of force models developed in literature with the purpose to describe their different characteristics (Section 3), particular attention has been paid to key issues for mechanistic models as the calibration and validation procedures. The main idea of mechanistic models is to calibrate on a small amount of experiments to predict forces in a large process operating window. Specific literature does not deal with the effects of the selected amount and position of calibrating tests in the operating window, i.e. the space of parameters where the process works correctly, and the objective evaluation of the model performance. The main purpose of this paper is to demonstrate how the calibration window selection affects the model prediction performance. For this reason, calibration experiments should be considered carefully when applying a mechanistic model.

2 Objectives

Main target of the presented research is to point out the relevance of the model calibrating conditions on the model prediction errors. In order to achieve this target, different important issues have been addressed:

- The force acquisition experimental procedure has to be carefully designed since the model prediction performance strictly depends on the calibration force signals accuracy (Section 5)
- A model prediction error index has to be defined in order to correctly assess the model performance in function of the calibrating window selection (Section 6)
- The model validation procedure has to be objectively defined to make it repeatable and allow comparisons among different calibration window performances (Section 7).

3 Literature review

Predictive models of machining operations can be classified in four main groups: analytical, numerical, empirical and semi-empirical models [1-6]. All these models allow to predict several fundamental process variables, such as chip thickness, cutting forces (which are the focus of the present paper), stress, strains, friction, and temperatures.

When machining in the microscale, analytical modeling is very complicated due to the microscopic features of the occurring phenomena, making the process observation and measurement difficult to carry out. Moreover, the cutting process mechanics becomes more complex to understand than in the macroscale, since typical phenomena such as the "minimum uncut chip thickness" effect take place [3-4, 7-8].

Due to these analytical modeling issues, many researchers represented the chip removal process in the microscale by means of numerical models based on Finite Elements Method (FEM) [9-12] or Molecular Dynamics (MD) [13-15]. These models rely on strong assumptions regarding the target material behavior: FEM is typically based on the isotropic material hypothesis, while the material microstructure is very influent when machining in the microscale. On the other hand, MD simulation is able to represent microscale phenomena but

it is often limited to deal with nanometer or angstrom scale fields due to the required huge computational power.

Strictly empirical models relate process parameters as feed, width of cut, depth of cut and cutting speed to the measured process performance of interest (e.g. cutting forces) by means of equations fitted to experimental data. These models are not general, since they are only capable to describe the experimental conditions for which they have been developed.

In order to gain more generality, semi-empirical or mechanistic models have been introduced both for the macro and the micro scale [16-37]. These models predict cutting forces by means of relationships containing empirically determined cutting coefficients and chip geometrical parameters that, in turn, are analytically obtained from the process kinematics. The empirical cutting coefficients allow taking into account the cutting phenomena that can be neither analytically modeled nor measured during the experimental tests.

The mechanistic models can be classified according to the type of experiment needed for calibrating the cutting coefficients.

The first group includes models based on the "unified mechanics of cutting" [16-24], whose coefficients are determined by simple orthogonal cutting tests where workpiece and tool materials are the same as those involved in the force prediction. Such coefficients are used to predict cutting forces for every tool geometry thanks to the analytical relationships between orthogonal and oblique cutting. These models do not need a large experimental effort as their empirical input is taken from a "standard" orthogonal cutting database.

Models describing the chip formation process by means of the orthogonal cutting slip-line field theory and linking to the milling process by a proper chip thickness analytical function can be included in this first group of semi-empirical models. This approach has been used in the studies of Jun et al. [38-40] and Altintas et al. [41], which are respectively based on the slip-line field models by Waldorf et al. [42] and Jin et al. [43-44].

The second group of mechanistic models includes models whose coefficients are determined by milling tests for each given cutter geometry and tool-workpiece material combination [25-37]. Within this group, several milling force prediction models, both for the macro [25-30] and for the micro scale [31-33], assume that the cutting coefficients depend on the average chip thickness and calculate them through the measured force average value. This fact leads to a low accuracy in the force peak values prediction, due to the difference between the actual and the average chip thickness. Moreover, the average coefficients should be determined through a great amount of tests in different experimental conditions since they are strongly related to process parameters (namely, feed rate, axial and radial depth of cut). In their studies about cutting force prediction for conventional end-milling and ball-end-milling, Yucesan et al. [34] proposed moving average cutting coefficients, which should be more efficient and accurate than the simple average coefficients. Ko et al. [35-36] introduced cutting-condition-independent coefficients, which reduce the experimental effort for the model calibration and lead to a more accurate cutting force prediction. Lee et al. [37] used cutting-condition-independent coefficients in their model for cutting force prediction in micro-end-milling, which deals with the size effect thanks to the partial effective rake angle introduction.

A mechanistic force model belonging to the second group has been selected from the macro- and micro-milling literature for the aims of this study. It is important to underline that the optimal model selection is not the target of the present study, but a suitable and representative force prediction model is needed to correctly and accurately capture the micromilling phenomena. The second mechanistic models group, that relies on milling tests for each given cutter geometry and tool-workpiece material combination, and in particular the model of Lee et al. [37], that is based on cutting-condition-independent coefficients and partial effective rake angle concepts, appears both as a suitable and promising tool for predicting forces in micromilling with a low calibration experimental effort.

A brief description of the model by Lee et al. [37] is given in the following Section.

4 Model description

As previously said, the present paper deals with the model by Lee et al. [37], whose main characteristics are described in this Section.

4.1 Model reference system and symbols

The mill geometry, the coordinate system and symbols used by the model are depicted in Figure 1. The force model splits the mill into "disk elements" perpendicular to the mill axis: this characteristic allows the model to follow the real mill edges geometry according to the local helix angle θ_h. Also the uncut chip thickness t_c is split into "slices" in order to calculate the partial effective rake angle $\alpha_{r,e}$. The thickness of disk elements and slices can be selected by the user; low thickness values improve the model accuracy. The partial effective rake angle allows to consider the typical micromachining size effect, which consists in a chip formation largely due to the ploughing action of the cutting edge radius r_e on the workpiece. The partial effective rake angle $\alpha_{r,e}$ is negative along almost all the edge radius r_e, producing high values of cutting force coefficients K_n and K_f. K_n and K_f are respectively calculated along the local rake face normal and along the tangent to the rake face, where the chip flows with an angle θ_c (chip flow angle) with respect to the horizontal plane. K_n and K_f coefficients are the cutting pressures that allow to calculate the force components F_n and F_f, acting along the same directions. The F_n and F_f resultant force is named R and can be decomposed in the force components F_x, F_y and F_z acting on the tool along the machine tool axes. The model predicts these latter components. A detailed description of the model equations can be found in [37].

4.2 Model implementation

A brief description of the model implementation is given in this Section. The model is organized into two operating phases, the "calibration phase" and the "prediction phase", both implemented in modules. The calibration phase fits real milling experimental data with Weibull functions to relate the cutting force coefficients (K_n and K_f) to the uncut chip thickness t_c. The logistic function is used to relate the chip flow angle θ_c to the angular position of each cutting edge θ (Equations 1-3) [37]. The model applies these functions, which seem to correctly represent the behaviours of the modelled quantities, to predict the cutting forces in the prediction phase.

$$K_n\left(t_c\right) = e^{\left(A_1-\left(A_1-A_2\right)\cdot e^{\left(-\left(A_4\cdot t_c\right)^{A_3}\right)}\right)} \tag{1}$$

$$K_f\left(t_c\right) = e^{\left(B_1-\left(B_1-B_2\right)\cdot e^{\left(-\left(B_4\cdot t_c\right)^{B_3}\right)}\right)} \tag{2}$$

$$\theta_c\left(\phi\right) = \frac{\left(C_1-C_2\right)}{1+\left(\phi \big/ C_3\right)^{C_4}} + C_2 \tag{3}$$

where ϕ is the angular position of a disk element at the cutting edge angular position θ, taking into account the helix angle θ_h [37]. A_i, B_i and C_i are respectively the parameters of the normal cutting force coefficient function, the frictional cutting force coefficient function and the chip flow angle function [37].

Cutting coefficients determined by the model calibration phase are independent from the cutting conditions such as width of cut a_e, depth of cut a_p, spindle speed n, cutting speed v_c and feed f_z. This feature makes the model able to predict forces for different process parameter combinations once a small set of calibration experiments is performed. However, calibration experiments have to be repeated each time the couple mill-target material varies.

In the present study, the calibration procedure has been designed to allow the acquisition of experimental force data from more than one mill revolution in order to improve the statistical significance. As a matter of fact, the implemented calibration procedure is based on five complete mill revolutions (Section 7.2).

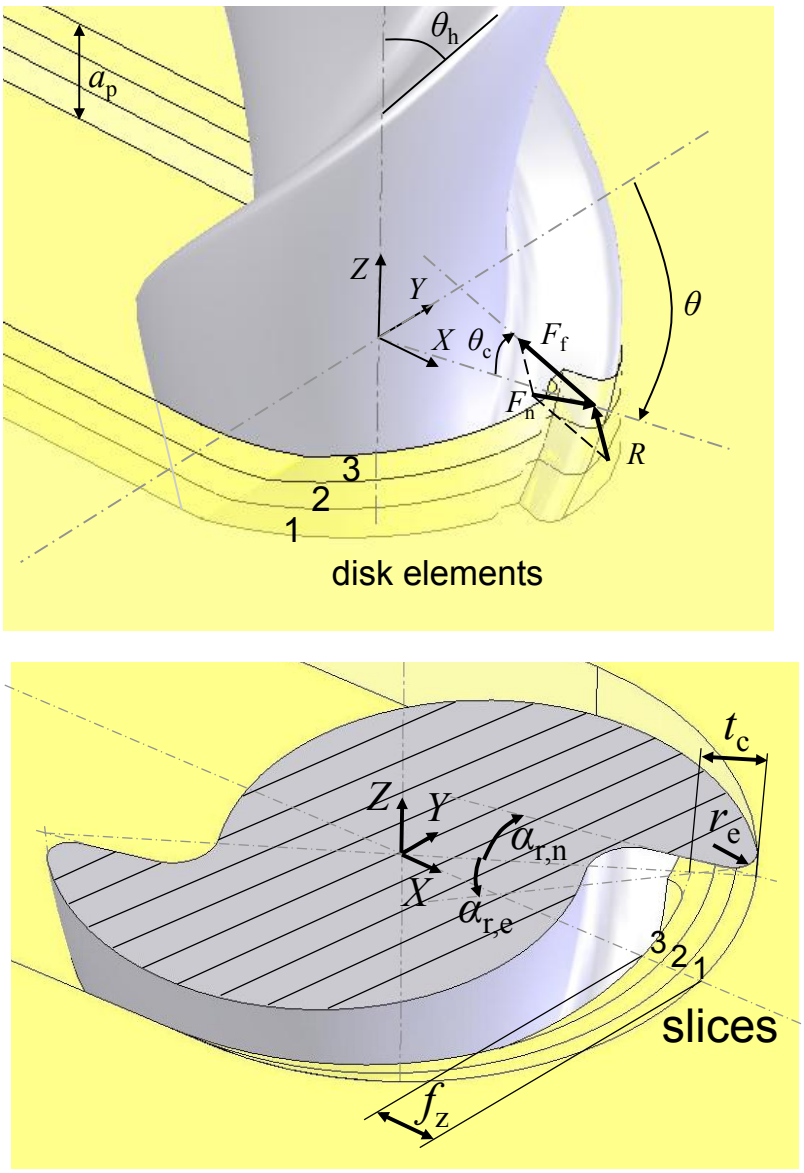

Figure 1. Model reference system and symbols [37]

5 Force acquisition experimental procedure

The force acquisition is a key aspect of the model calibration phase. Milling forces are characterized by a complex spectrum of harmonics due to the discontinuous nature of this process [45]. Spindle frequency and tooth passing frequency contain most of the signal power, but are not sufficient to reproduce the milling force signal shape in the time domain, which is fundamental when dealing with cutting force modeling.

The model calibration counts on correctly acquired force signals in order to maximize the model prediction performance. First step in this direction is to measure forces by a large bandwidth load cell. Top piezoelectric load cells on the market, as the one employed in this study (Kistler 9317B), can count on a limited bandwidth, which is not enough to correctly acquire the micromilling force signal at high spindle rotational speeds (50000 rpm and more for current micromilling centers). Some harmonics are amplified by the load cell dynamic behavior and the acquired signals are consequently distorted.

Under the hypotheses of system linearity, single degree of freedom, limited cross-talk among different force directions and time independence of the identified modal parameters, the dynamic effects of the system (composed by dynamometer, workpiece and fixtures; see also Table 1) on the acquired forces can be compensated by determining its frequency response function (*FRF*) and consequently the experimental filters to apply to acquired forces in order to obtain compensated forces. The hypothesis of single degree of freedom is suitable for the present case since *X* and *Y FRF* amplitudes are unitary until the measured first resonance frequency of the workpiece-dynamometer-fixtures system (which can be identified by a SDOF model) and are almost equal to zero for higher frequencies.

The force compensation approach has been implemented in this study through the following steps:

- Impact test (*X* and *Y* axes) at the specimen fixtured on the dynamometer (steel tip impact test hammer PCB 086E80; acquisition board NI9234, chassis cDAQ-9178; sampling frequency: 25600 Hz; anti-aliasing filter cut-off frequency: 11500 Hz; acquisition time: 1 s)
- Calculation of *X* and *Y* experimental *FRF*s as the ratio in the frequency domain between the force measured by the dynamometer and the force acquired by the hammer during the impact test
- Verification of the system linearity hypothesis through the coherence between the force measured by the dynamometer and the force acquired by the hammer
- *X* and *Y FRF* modal parameters identification by means of the single degree of freedom model
- *X* and *Y FRF* inversion to obtain the experimental filters needed to compensate *X* and *Y* acquired forces

F_z has not been compensated since it is less informative and the dynamometer bandwidth is higher in that direction.

This approach allows eliminating unwanted dynamic effects and, at the same time, to preserve harmonic components located at higher frequencies than the nominal dynamometer bandwidth. Moreover, the measurement noise is not amplified since the acquired signals are compensated by the identified FRFs and not by the experimental ones. The advantages of using this compensation method have been evaluated by comparing unfiltered, low-pass filtered and compensated forces at different cutting speeds, feeds and widths of cut.

Figure 2(a) shows a comparison among measured, compensated and low-pass filtered forces in the time domain (cutting conditions reported in the figure caption); Figure 2(b) shows a comparison among the measured, compensated and low-pass filtered F_x components in the frequency domain (same conditions of Figure 2(a)), together with the acquisition system *FRF* along the *X* axis.

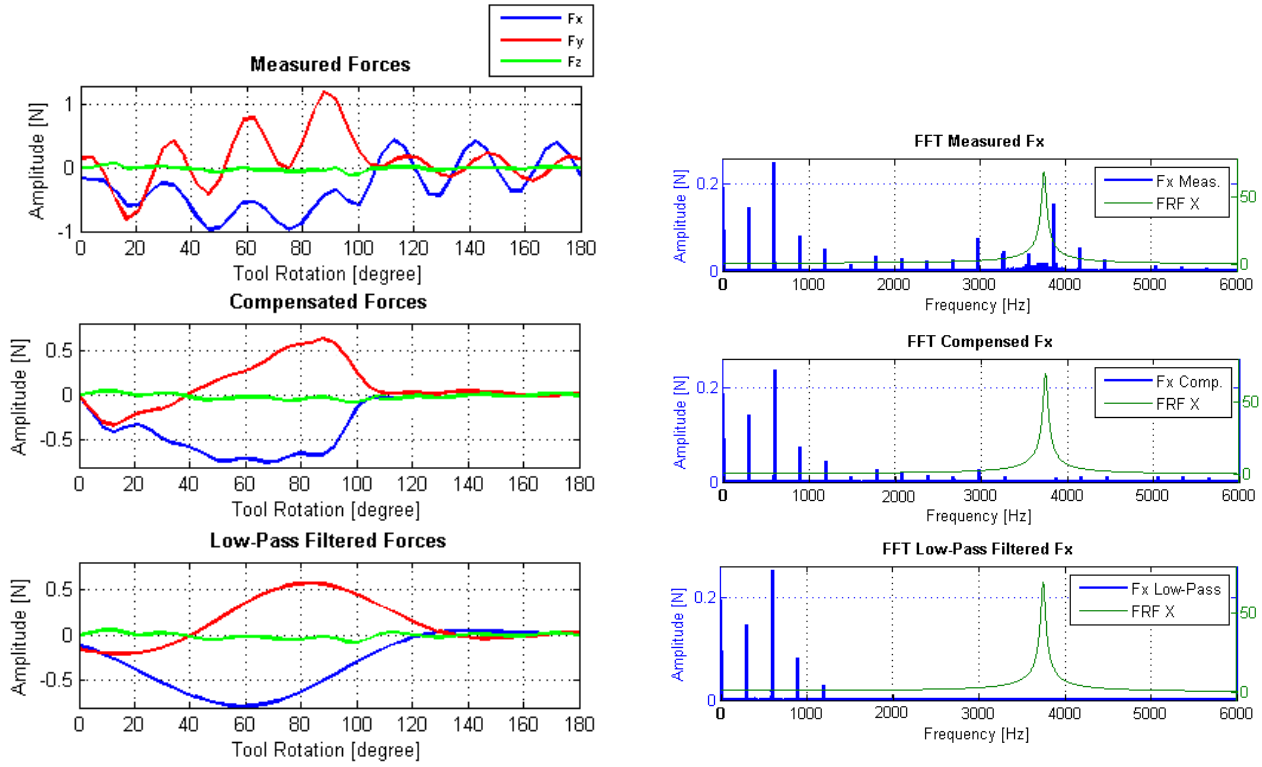

(a) (b)

Figure 2: Comparison between measured, compensated and low-pass filtered cutting forces. a) time domain; b) frequency domain. (mill: Dormer S150.5; D = 0.5 mm; I = 2; r_e = 4 µm; $\alpha_{r,n}$ = 0°; θ_h = 30°; workpiece: Aluminium 6082-T6; cutting parameters: a_p = 0.05 mm; a_e = 0.25 mm (only one cutting edge engaged at the same time); f_z = 4 µm; v_c = 27.85 m/min; n = 17730 rpm; milling approach: up-milling; f_s = 25600 Hz; anti-aliasing filter cut-off frequency = 11500 Hz; 5th order Butterworth low-pass filter cut-off frequency = 6000 Hz (in case of measured and compensated forces); 1300 Hz (in case of low-pass filtered forces))

Regarding the filtering approach, the applied 5th order Butterworth low-pass filter cut-off frequency has been set to 1300 Hz, according to the sensor bandwidth specifications reported in the Kistler© 9317B dynamometer user manual [46]. This cut-off frequency corresponds to the value at which the measuring system frequency response function applies a 10% amplification on the harmonics modulus. The top graph of Figure 2(b) clearly shows the F_x signal dynamic distortions taking place near the system first natural mode; the related high

frequency vibrations can be seen in the time domain in the top graph of Figure 2(a). The compensation approach reduces this amplitude distortion preserving enough information to reconstruct the signal up to 6 kHz, while the low-pass filter removes the harmonics above 1300 Hz. In both cases, the tooth passing frequency stays within the bandwidth of the low-pass filter, but the compensated forces have a higher definition than the filtered ones. The tool engagement and disengagement phases, as well as the signal shapes, cannot be correctly estimated using low-pass filtering.

It should be highlighted that the compensation method based on the frequency response function inversion, as well as other available approaches based on the measuring system dynamic behaviour evaluation [47], is highly dependent on the hypotheses of linear behaviour and time independence of the system dynamic characteristic. System linearity has been proved, but some material is removed from the workpiece mounted on the dynamometer during the machining process, therefore the force measuring system mass decreases, making it not strictly time independent. Anyway, the material amount removed in each micromilling test is about the 0.4% of the total workpiece mass, hence the mass time independence can be considered acceptable, making the proposed compensation approach a suitable method to eliminate the unwanted dynamic effects in the studied bandwidth.

A last note regarding the use of load cells like the Kistler 9317B is needed. As this cell has only one triaxial sensitive piezoelectric element at the cell center, the force measurement is sensitive to the distance of the force application point from the cell center. For this reason, a preliminary study has been carried out to verify that in case of the selected specimen geometry (Section 7.2), this kind of error is negligible.

6 Objective model prediction error definition

A second key topic for both the force prediction model calibration and validation is the definition of its performance in terms of the difference between measured and predicted cutting forces. The force model performance is usually evaluated by means of a graphical comparison in the specific micromilling literature: such a qualitative approach does not lead to an objective evaluation of the model performance.

The present study proposes a quantitative analysis of the model prediction error based on the root mean square error index (*RMSE*), as show in Equation 4:

$$RMSE_i = \sqrt{\frac{\sum_{j=1}^{N}\left(F_{i,\text{meas}}(j) - F_{i,\text{pred}}(j)\right)^2}{N}} \qquad i = x, y, z \qquad (4)$$

where i is the machine tool axis index, $F_{i,\text{meas}}$ and $F_{i,\text{pred}}$ are respectively the measured force and the predicted force component along the i^{th} machine axis in a certain experimental condition, N is the total amount of acquired points available for each force component over a certain number of tool revolutions, and j is the acquired force point index.

Both measured and predicted forces have to be sampled with the same sampling frequency to correctly estimate the *RMSE* (Section 7.1).

The number of consecutive tool revolutions to extract from the measured and predicted force signals to calculate the *RMSE* can be set by the user, exactly as it is possible to do regarding the number of revolutions to use for the model calibration (Section 4.2). This fact allows the model calibration and validation to be more robust to the process variability.

In the present study, *RMSE* has been calculated for each condition of the carried out experimental plan (Section 7.1) over five complete tool revolutions.

Acquired forces have demonstrated to be very stable over the five considered periods, thanks to the correct parameters and conditions selection. This way, high *RMSE* values can be definitely associated to differences between acquired and predicted forces and not to a large variability of the process itself.

7 Validation procedure and calibration window selection

As already mentioned, one interesting characteristic of mechanistic models is the possibility to calibrate them on a small amount of experimental tests. In order to achieve the best results, it is important to know if the force prediction performance is affected by the number of calibration tests and their position inside the process operating window. This is the main objective of the present study.

If different calibration windows have to be compared in terms of model prediction performance, a model validation procedure is needed, i.e. a method to objectively evaluate such a performance. The *RMSE* index defined in the Section 6, comparing measured and predicted forces, can be applied with this aim to all the conditions of the process operating window, which is the space of all possible process parameters combinations, once the model is calibrated in a specific calibration window, which is the space of the process parameters combinations used to calibrate the model. The obtained model error maps can be compared in order to determine the best calibration window and the *RMSE* mean value calculated over the whole process operating window can be used as synthetic model performance index.

The present study has carried out a comprehensive experimental campaign to set-up a data base corresponding to the process operating window. The present Section describes this experimental plan and the model prediction performance corresponding to different calibration windows selections inside the process operating window.

7.1 Experimental plan

The calibration and validation experimental plan has been defined on parameters playing a stronger role on the machining operation and on the cutting force measurement and dynamic compensation (Table 2). This Section describes the role and effects of each model parameter with the aim to define the experimental plan to carry out to obtain the mentioned experimental conditions data base.

Mill geometrical parameters

The TiAlN coated hard metal Dormer S150.5 mill (D = 0.5 mm; I = 2; r_e = 4 μm; $\alpha_{r,n}$ = 0°; θ_h = 30°) has been selected for the present study. This tool has been employed at MI_crolab of Dipartimento di Meccanica of Politecnico di Milano in previous researches [48].

Workpiece material

Aluminium 6082-T6, a structural alloy commonly used for machining, has been selected for the present study since it is a representative material, widely used in literature.

Depth of cut

The depth of cut a_p upper limit has been set according to some indications on microtools load strength coming from literature. Kim et al. [49] suggested a maximum depth of cut equal to 20% of the mill diameter to avoid tool breakage due to an excessive load. Such an indication is coherent with manufacturer catalogues. The depth of cut lower limit should be selected basing on the ratio between the major and minor cutting edge engaged lengths. Since the force prediction model is not able to simulate the minor cutting edge effects, it is better to avoid process conditions where the influence of this cutting edge can be relevant. Additionally, a very low depth of cut can cause excessive localized tool wear due to the occurring cutting edges

ploughing and rubbing actions. Basing on these considerations, a depth of cut lower limit equal to 10% of the mill diameter seems to be reasonable.

Width of cut

The width of cut a_e is often expressed as a function of the tool diameter (a_e/D). The cutting force coefficients calibration tests are characterized by only one engaged cutting edge at a time since the model calibration phase could not distinguish actions of different cutting edges working simultaneously (this is not the case for the prediction phase, that uses the superposition principle). Moreover, the uncut chip thickness has to range between zero and the feed per tooth in calibration tests. This fact requires a_e/D equal or greater than 0.5. This way, there are enough points to fit the curves relating the cutting force coefficients (K_n and K_f) to the uncut chip thickness t_c (Equations 1-2). It has been decided to fill the a_e/D range up to its maximum value (equal to 1 and corresponding to a full slotting operation) with another level (0.75) to have the possibility to evaluate different calibrating windows.

Feed

This parameter, together with the cutting speed, is the main factor affecting the tool wear and the machined surface quality. Feed is also crucial in micromilling since it influences the minimum chip thickness phenomenon, i.e. the ploughing action taking place instead of chip formation when the instantaneous chip thickness value is lower than a critical value [4, 37]. The minimum chip thickness depends on the cutting edge radius and the workpiece material [8] (e.g. it is approximately the 30% of the tool edge radius for aluminium alloys [49]). Therefore, a different feed lower limit should be set for each tool-workpiece combination to prevent situations where the ploughing action affects most of the tooth engagement angle, leading to tool vibrations and bad surface quality. The feed factor is expressed in terms of ratio

between the feed itself and the nominal cutting edge radius (f_z/r_e) since this formulation is effective in indicating whether the chip flows mainly on the cutting edge radius ($f_z/r_e < 0.30$) or also on the rake face ($f_z/r_e > 0.30$), allowing a direct comparison with the minimum chip thickness threshold. Critical conditions, where the ploughing action is predominant comparing to the shearing action along the tooth engagement angle, have been avoided in the experimental design by selecting f_z/r_e ranging from 0.5 to 1. A lower value of 0.5 ensures that the instantaneous uncut chip thickness ranges from zero to a value higher than the 30% of the cutting edge radius along the tooth engagement angle and that the cutting action passes certainly from ploughing to shearing. It is reasonable not to overcome the upper limit of 1 to avoid excessive mill loads.

Cutting speed

Finding the appropriate cutting speeds (v_c) in micromilling is often challenging since values suggested by catalogues are usually obtained by extrapolating macro cutting conditions. This procedure carries out too high cutting speeds for the thermal actions allowed in micromachining and for the current spindles capabilities. The workpiece microstructure [38], the minimum chip thickness effect and the other microscale machining typical phenomena increase the thermal effects in the tool-workpiece contact region, thus the approach to select cutting speeds should be different from the macroscale.

Additionally, v_c is related to the sampled force angular pitch $\Delta\theta_s$ (Equation 5): the higher v_c and n are, the higher the force frequencies; this fact requires higher force sampling frequencies f_s to maintain a defined $\Delta\theta_s$, but the available force acquisition system bandwidth sets an upper limit to this trend (Section 5).

Preliminary experiments have been carried out to find out proper cutting speed values for the selected tool-workpiece couple. The cutting speed range shown in Table 2 allows a

sufficient number of cutting force harmonics (at least 20) to stay within the available compensated bandwidth (Section 5), to generate an acceptable workpiece surface quality and to determine a fine $\Delta\theta_s$ (Section 7.2). It should be noted that this study does not aim at investigating the effect of milling parameters on cutting forces, hence it is not needed to explore the whole range of suitable process parameters for the selected milling operations. v_c values in Table 2 correspond to spindle rotational speeds of 8850 and 17850 rpm.

Moreover, each combination of depth of cut and cutting speed has been checked in order to be a chatter free cutting condition.

Table 1: Experimental set-up and acquisition system

Machine tool	Kern EVO CNC ultra-precision 5-axis machining centre (spindle speed up to 50.000 rev/min, nominal positioning tolerance = ±1 □m, precision on the workpiece = ±2 □m)
Dynamometer	Piezo-electric tri-axial dynamometer Kistler 9317B
Charge amplifiers	Kistler 9015A
Acquisition board	NI 9234; sampling frequency (f_s) = 25600 Hz; anti-aliasing filter cut-off frequency = 11500 Hz
Data filtering	5^{th} order Butterworth low-pass filter cut-off frequency = 6000 Hz

Table 2: Micro-end milling force prediction model parameters

Mill parameters (constant)					
Symbol	**Parameter**	**Unit**	**Value**		
-	mill material	-	TiAlN coated hard metal		
D	mill diameter	mm	0.5		
I	number of flutes	-	2		
r_e	cutting edge radius	µm	4		
$\alpha_{r,n}$	nominal rake angle	degrees	0		
λ_h	helix angle	degrees	30		
-	milling approach	-	up-milling		
	feed direction		X		
Workpiece parameters (constant)					
Symbol	**Parameter**	**Value**			
-	workpiece material	Aluminium 6082-T6			
Process parameters (variable)					
Symbol	**Parameter**	**Unit**	**Value**	**Non dimensional value**	
a_p	depth of cut	mm	0.05, 0.075, 0.1	a_p/D	0.1 – 0.15 – 0.2
a_e	width of cut	mm	0.125, 0.250, 0.375, 0.500	a_e/D	0.25 – 0.5 – 0.75 – 1
f_z	feed per tooth	µm	2, 3, 4	f_z/r_e	0.5 – 0.75 – 1
v_c (n)	cutting speed (spindle rotational speed)	m/min (rpm)	13.90 (8850), 28.04 (17850)	-	-

Summing up, the proposed experimental design is a complete factorial plan composed of 72 process parameter combinations and 2 replicates for a total amount of 144 runs, which have been completely randomized. The experimental plan conditions are summarized in Table 2. Such conditions conventionally define the process operating window in the frame of this paper. One mill has been used to carry out all the experimental runs; the limited total cutting time has made the tool wear effects negligible, as confirmed by visual analyses of the cutters at the microscope.

The three force components (F_x, F_y and F_z) have been selected as responses of the experimental plan (see Section 5 for force compensation and Section 7.2 for force elaboration).

7.2 Experimental set-up and data elaboration

The experimental plan described in Section 7.1 has been performed using the experimental set-up and acquisition system described in Table 1.

Figure 3 represents the used specimen and the mill ready to produce the first trial. Slots have been prepared before carrying out the three hosted experimental trials in order to exclude set-up errors which could affect a_p and a_e. A total number of 48 specimen has been used in this study.

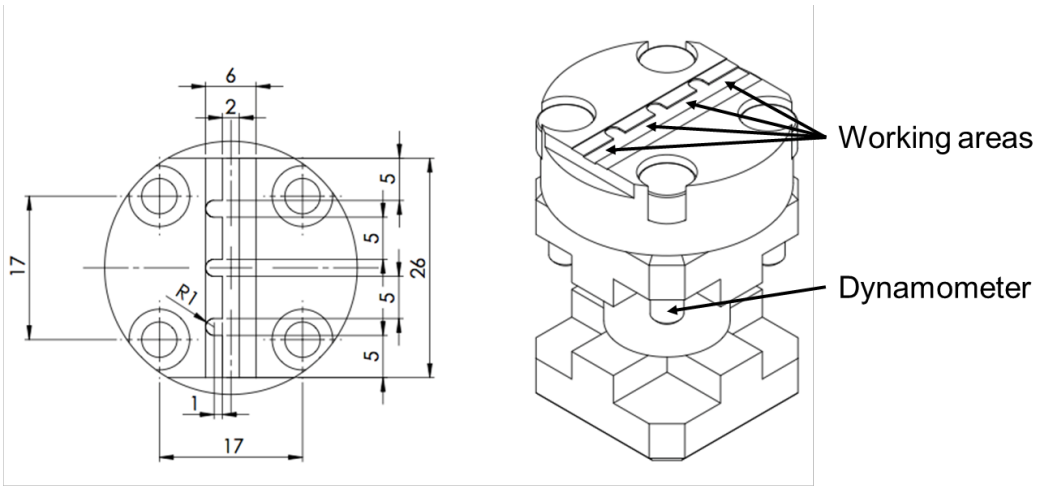

Figure 3: Specimen mounted on the dynamometer

LabVIEW© has been used both for data acquisition and for the force model implementation.

As already said in Section 5, the force signal bandwidth is limited by the applied dynamometer and the specimen mass. The force compensation procedure allows to extend the available bandwidth to 6 kHz; the force sampling frequency and the filters cut-off frequencies have been set according to this value (Table 1). Together with n, the force sampling frequency f_s (Table 1) defines the angular pitch between acquired force points according to the Equation 5:

$$\Delta\theta_s = \frac{360 \cdot n}{60 \cdot f_s} \qquad (5)$$

$\Delta\theta_s$ is equal to 2.07° for n = 8850 rpm and 4.18° for n = 17850 rpm. These angular pitch values are very important since the part of the model that calculates the cutting edges kinematics, both in the calibration and in the prediction phases, has to use the acquired force pitch for reducing errors.

The force compensation algorithm needs a rational frequency resolution for the input signals: this way, it has been decided to produce force signal time windows exactly 5 s long to obtain a frequency resolution equal to 0.2 Hz and consequently also a good spectral information. The actual spindle rotational speed has been used to calculate the number of complete tool revolutions contained in a 5 s time window; the points needed to complete the time window have been set to zero according to the zero padding technique. The rational frequency resolution does not allow to eliminate leakage, but the whole procedure makes it acceptable.

Every force time window has been then compensated according to the procedure explained in Section 5 and further windowed and phased with the model angular reference system in the time domain in order to exactly extract 5 tool revolutions.

The obtained data base of force signals, corresponding to conditions of the process operating window, have been made available for the following performance analysis of different calibration windows (Section 7.3). It has to be pointed out how the data base produced in this study has not the purpose to precisely define the process operating window, but to representatively cover it in order to contain a large variety of different admissible working conditions.

7.3 Model performance sensitivity to the calibration window selection

A statistical analysis of the model prediction performance sensitivity to different calibration windows has been carried out in this Section.

The calibration window can be defined as a small set of experimental conditions selected in the process operating window to calibrate the model.

Force signal files (containing the five tool revolutions elaborated according to the procedure described in Section 7.2) have been loaded in the model calibration procedure for each one of the tested calibration windows in order to fit the functions of the cutting force coefficients (K_n and K_f) and the chip flow angle θ_c (Equations 1-3). K_n and K_f depend on t_c and θ_c depends on θ in this fitted functions. Fitting coefficients are the calibration phase result and the input to the model prediction phase. The model performance has been evaluated over the whole operating window. It is worth to remind how, comparing to the literature, the presented procedure takes into account process variability considering more than one tool rotation for calibrating purposes.

Next Sections deal with the three calibration windows studied in the present paper: the "complete" one (the most comprehensive calibration window), the "reference" one (taken from the reference literature) and the "suggested" one (found out in the present study as an improvement of the previous ones).

The complete calibration window

Not all the experimental conditions of the conventional process operating window defined in this paper, and represented in Table 2, can be used for calibrating purposes. The characteristics needed for an experimental condition to be part of the calibration window are:

- Only one cutting edge has to be engaged at the same time ($a_e/D < 1$) (Section 7.1)
- The cutting edge has to be engaged for at least 90 degrees ($a_e/D \geq 0.5$) in order to pass through all the uncut chip thickness values from zero to the maximum (corresponding to the feed per tooth f_z)

- The current version of the model cannot be calibrated by forces affected by tool runout. Since runout produces peaks of different heights for the two cutting edges, it has been decided to always consider the part of the force signals produced by the most engaged cutter (the highest one) for calibration purposes. This cutter follows a trajectory that is more similar to the nominal cycloid, hence Equations 1-2 can be successfully fitted on experimental data.

The complete calibration window is composed by all the conditions of the process operating window (Table 2) which satisfy these constraints. This window is the widest one, with 36 experimental combinations repeated two times, for a total of 72 employed force signals (Table 3). Such a wide window is not coherent with the purpose to calibrate the model on a small series of experiments, but it is useful for the next comparisons carried out in this paper.

Table 3: "Complete" calibration window

Process parameters				
Symbol	**Unit**	**Value**	**Non dimensional value**	
a_p	mm	0.05, 0.075, 0.1	a_p/D	0.1 – 0.15 – 0.2
a_e	mm	0.250, 0.375	a_e/D	0.5 – 0.75
f_z	µm	2, 3, 4	f_z/r_e	0.5 – 0.75 – 1
v_c (n)	m/min (rpm)	13.90 (8850), 28.04 (17850)	-	-

Fitting coefficients for the K_n and K_f and θ_c functions have been obtained by the model calibration over this calibration window (Section 4.2). Such coefficients have been employed in the prediction phase to obtain predicted forces for all the process parameters combinations included in the process operating window (Table 2).

The *RMSE* has been calculated for all the three force components by comparing measured and predicted forces obtained in the same conditions over the entire process operating window. A proper statistical analysis showed how the F_z component mean *RMSE* calculated over the whole process operating window has been always approximately one order of magnitude lower than F_x and F_y components mean *RMSEs.* Moreover, $RMSE_x$ and $RMSE_y$ proved to be highly correlated between each other. These results have allowed to focus the following analysis only on $RMSE_x$. The same considerations are valid also for the reference and the suggested calibration windows.

The regression model reported in Equation 6 has been obtained after coding each process parameter value as -1 when equal to the lowest end of the process operating window range (Table 2) and as 1 when equal to the highest end (intermediate coded values have been proportionally calculated): this way, each regression equation coefficient directly represents the process parameter weight on the $RMSE_x$.

$$\sqrt{\mathrm{RMSE}_{\mathrm{x,complete}}} = 0.384 + 0.00075 \cdot v_c + 0.0279 \cdot f_z + 0.102 \cdot a_e + 0.0680 \cdot a_p + 0.0410 \cdot f_z \cdot a_e \qquad (6)$$

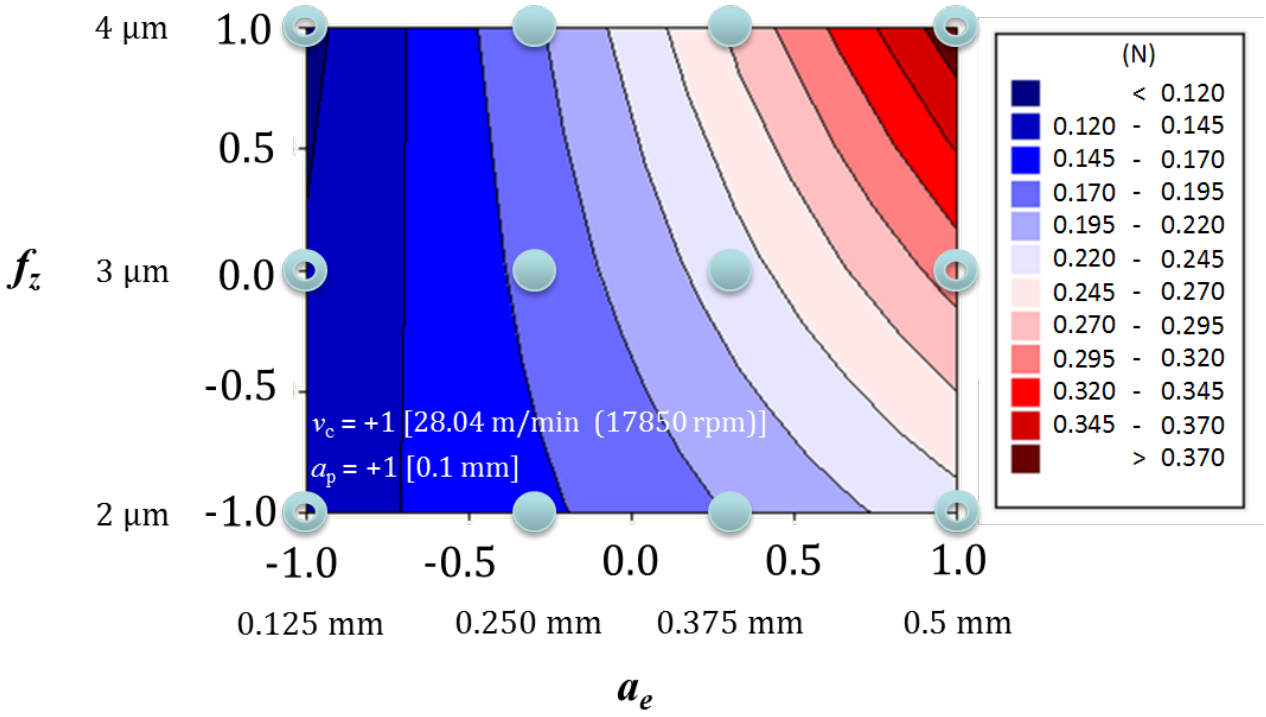

Figure 4: $RMSE_{x,\text{complete}}$ map at v_c = +1 (28.04 m/min (17850 rpm)) and a_p = +1 (0.1 mm). Solid dots represent points where both calibration and validation have been carried out. Empty dots represent points where only validation has taken place

The regression model fully satisfies the analysis of variance (ANOVA) hypotheses of normality distribution, equal variances and time independence of residuals [50]. Moreover, it is statistically significant and its R^2_{adj} [50] is equal to 84% as an indication of how good this model explains the observed data variability. The cutting speed v_c is not significant, as confirmed by its low regression coefficient, but it has been included in the model to pass the lack of fit test [50]. The non significance of v_c confirms the model hypothesis according to which v_c does not play a role on forces, even if it cannot be excluded that higher cutting speeds could induce sufficient thermal effects to act on the cutting force coefficients. The regression model is basically additive and the most influencing cutting parameters are the depth of cut a_p, the width of cut a_e, the feed per tooth f_z and their interaction.

Other models have been fitted to experimental data, but the model containing only first degree terms, apart from the $f_z \cdot a_e$ second order mixed term, demonstrated to be both the most suitable under the statistic point of view and the simplest possible.

The sensitivity analysis points out how the $RMSE_{x,\text{complete}}$ model performance decreases as the process parameters increase, as indicated by the positive sign of regression coefficients in Equation 6. A graphical representation of the force prediction model performance $RMSE_{x,\text{complete}}$ in function of a_e and f_z when a_p and v_c assume the worst value is presented in Figure 4. In the graphical representation of $RMSE_x$ on the process operating window, it has been decided to pay more attention to the effect of f_z, a_e and their interaction since f_z and a_e are the core parameters used by the model to explain the force behaviour, while v_c has proved not to be significant and a_p plays a theoretically linear effect on the cutting forces.

A further analysis has been carried out on the $RMSE_x$ response divided by the mean value of the peak F_x moduli along the five acquired periods. Such an analysis is useful to check the significance of cutting parameters on a relative error index, where the error magnitude is considered relatively to the force magnitude, based on the principle according to which it is reasonable that higher forces could imply higher errors without affecting the model prediction performance. It is interesting to point out how the relative error maps show the same results reported in Figures 4-6, where higher cutting parameters values produce higher errors. Among the other cutting parameters, only a_p shows a different effect on the relative error respect to the absolute one. In fact, it is not significant on the relative error, thus demonstrating that the model substantially captures the direct effect of a_p on forces and that the error is directly related to the force magnitude.

The reference calibration window

The calibration window presented in this Section is the reference of this study since it has been applied, with some small differences explained in the following, by Lee et al. [37] to calibrate their mechanistic model.

Four process parameter combinations that satisfy the calibration constrains discussed for the complete calibration window have been selected to calibrate the cutting force coefficients; process parameters levels have been set at their lowest acceptable value excluding feed, that has been varied in each test (Table 4).

In order to cover a f_z/r_e range similar to the one used in [37], f_z = 5 μm has been added to the calibration conditions.

The applied cutting speed v_c has been lower than the one used by Lee et al. [37], which was equal to 15.8 m/min (n = 10000 rpm). This choice aims at avoiding the leakage caused by the irrational frequencies that would have characterized the cutting force main harmonics. A set of four experiments (one replication per condition) has been especially carried for this calibration window to guarantee homogeneous experimental conditions.

Table 4: "Reference" calibration window

Process parameters				
Symbol	**Unit**	**Value**	**Non dimensional value**	
a_p	mm	0.05	a_p/D	0.1
a_e	mm	0.250	a_e/D	0.5
f_z	μm	2, 3, 4, 5	f_z/r_e	0.5 – 0.75 – 1 – 1.25
v_c (n)	m/min (rpm)	13.90 (8850)	-	-

The same procedure described for the complete calibration window has been applied also in case of the reference calibration window to obtain predicted force components and *RMSEs* over the entire process operating window. Also in this case, it is worth focusing the analysis on only $RMSE_x$. The relative error ($RMSE_x$ divided by the mean value of the peak F_x moduli along the five acquired periods) shows the same trends as the absolute one in function of the process parameters. The process parameter a_p is significant on $RMSE_x$ while it is not on the relative error, as in the case of the complete calibration window. The regression model reported in Equation 7 has been obtained after coding the process parameters values as already described for the complete calibration window.

$$\sqrt{\mathrm{RMSE}_{\mathrm{x,reference}}} = 0.484 - 0.00222 \cdot v_c + 0.0624 \cdot f_z + 0.126 \cdot a_e + 0.0816 \cdot a_p + 0.0306 \cdot f_z \cdot a_e \qquad (7)$$

Also in this case, the model structure already used for $RMSE_{x,\mathrm{complete}}$ is the most suitable.

The regression model fully satisfies the ANOVA hypotheses, it is statistically significant and its R^2_{adj} [50] is equal to 86%. v_c is not significant inside the $RMSE_{x,\mathrm{reference}}$ regression model even if it has been kept to pass the lack of fit test [50].

The regression model is additive and a_p, a_e, f_z and the interaction between a_e and f_z play the major role on the force prediction model performance, which gets worse when process parameters increase. This last consideration is not valid for v_c, but its effect is negligible. A graphical representation of the force prediction model performance $RMSE_{x,\mathrm{reference}}$ in function of a_e and f_z when a_p and v_c assume the worst value is presented in Figure 5.

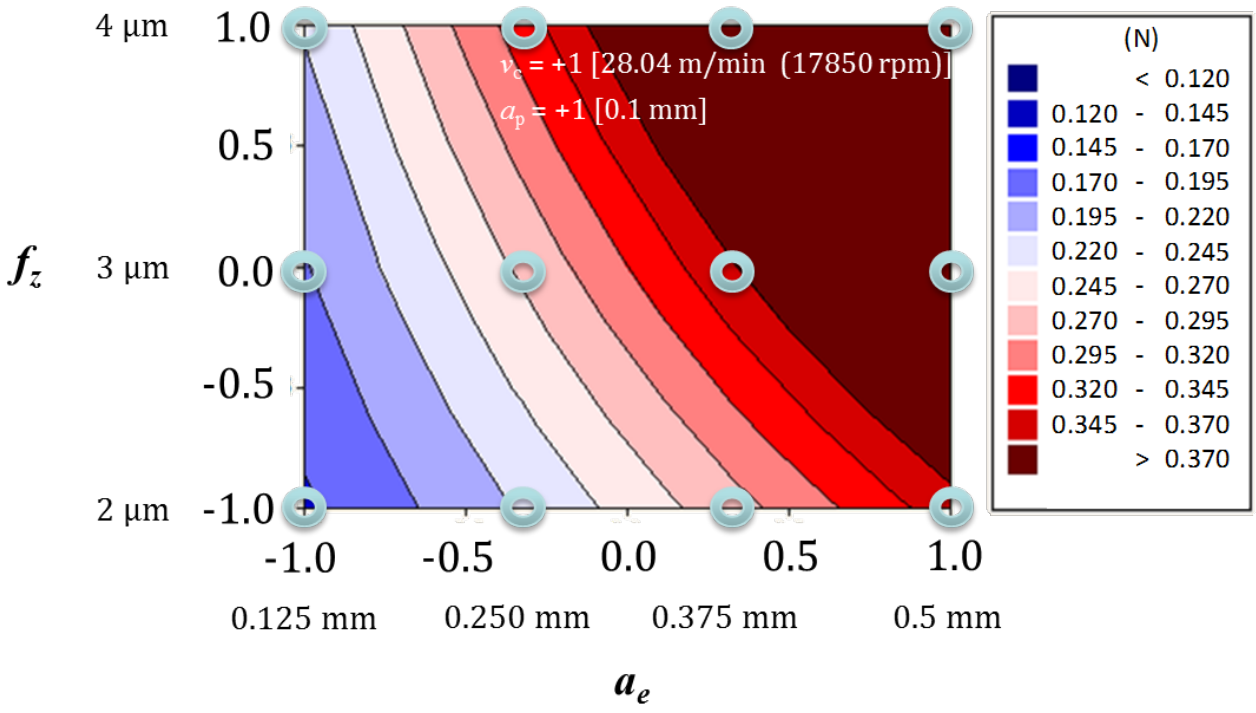

Figure 5: $RMSE_{x,\text{reference}}$ map at v_c = +1 (28.04 m/min (17850 rpm)) and a_p = +1 (0.1 mm). Empty dots represent points where only validation has taken place. No calibration points are visible on this plane

As it could be expected, the "complete" calibration window produces better predictions than the "reference" one since it calculates the fitting coefficients based on more data: the $RMSE_x$ mean value calculated over the whole process operating window is equal to 0.250 N for the reference calibration window and 0.157 N for the complete one.

The suggested calibration window

The complete calibration window performance has demonstrated to be better than the reference one even if it is not coherent with the aim of mechanistic models to minimize the experimental effort required for their calibration. This is the reason why this Section has been focused on determining a possible calibration strategy that maximizes the model prediction performance contemporarily reducing the required experiments. The proposed approach to

define the so called “suggested” calibration window is based on the general rule of thumb according to which the cutting quality tends to get worse when forces increase. This trend seems to be applicable also to the model force prediction performance, which is worse for both the tested calibration windows where cutting parameters assume their maximum value, i.e. where forces are higher. Only v_c should be excluded from this analysis since it is not significant on $RMSE_x$ and also on the cutting force. In any case, it is reasonable to consider an high value of v_c more critical, since it tends to produce process instabilities.

According to these assumptions, it seems advisable to calibrate the model in the most critical process operating window area. This way, process parameters highest values have been selected to form the suggested calibration window, always considering the calibration constraints already defined for the complete calibration window.

Three conditions with two replicates have been included, for a total amount of six milling tests (Table 5).

Table 5: “Suggested” calibration window

Process parameters				
Symbol	**Unit**	**Value**	**Non dimensional value**	
a_p	mm	0.1	a_p/D	0.2
a_e	mm	0.375	a_e/D	0.75
f_z	µm	2, 3, 4	f_z/r_e	0.5 – 0.75 – 1
v_c (n)	m/min (rpm)	28.04 (17850)	-	-

The $RMSE_{x,\text{suggested}}$ regression equation is expressed in Equation 8 and the error map in the worst conditions (v_c = +1 and a_p = +1) is depicted in Figure 6.

$$\sqrt{\text{RMSE}_{\text{x,suggested}}} = 0.391 + 0.00154 \cdot v_c + 0.0178 \cdot f_z + 0.0815 \cdot a_e + 0.0693 \cdot a_p + 0.0434 \cdot f_z \cdot a_e \quad (8)$$

The regression model fully satisfies the ANOVA hypotheses, it is statistically significant and its R^2_{adj} [50] is equal to 80%. Also in this case, v_c is not significant inside the $RMSE_{x,suggested}$ regression model even if it has been kept to pass the lack of fit test [50]. The most influencing factors are, as in the other cases, a_p, a_e, f_z and the interaction between a_e and f_z.

Also in this case, the model structure already used for $RMSE_{x,complete}$ and $RMSE_{x,reference}$ is the most suitable under the statistical point of view. The analysis of the relative error brings to the same results of the previous calibration windows. Also the relative error increases where the process parameters assume high values and it does not depend on a_p (see comments on the previous calibration windows).

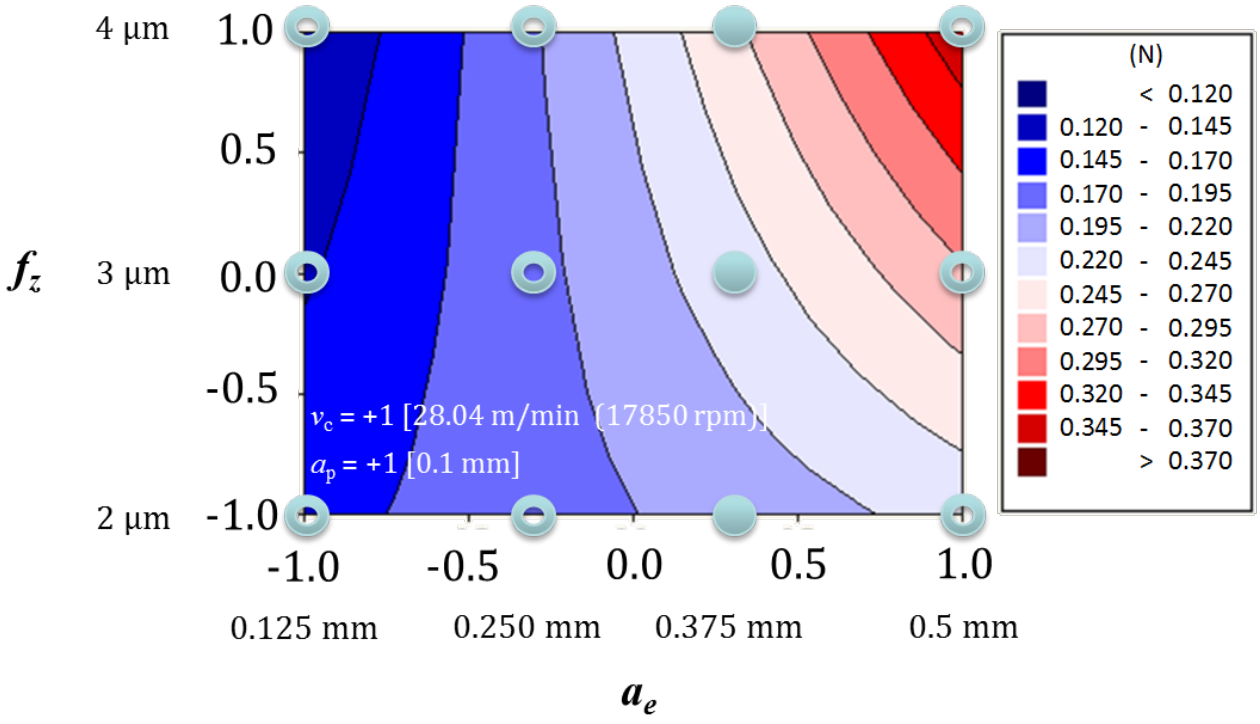

Figure 6: $RMSE_{x,suggested}$ map at v_c = +1 (28.04 m/min (17850 rpm)) and a_p = +1 (0.1 mm). Solid dots represent points where both calibration and validation have been carried out. Empty dots represent points where only validation has taken place

As it can be noticed from a comparison of Figure 4 and Figure 6 and from a comparison of Equation 6 and Equation 8, the model prediction performance in case of the suggested calibration window is similar to the one obtained from the complete calibration window. The $RMSE_x$ mean value calculated over the whole process operating window is equal to 0.161 N for the suggested calibration window and 0.157 N for the complete one.

8 Discussion

The best way to discuss results is to briefly summarize the steps performed in this study pointing out the related achievements:

- Three different calibration windows, composed by different combinations of the process parameters a_p, a_e, f_z and v_c, have been selected
- The model has been calibrated on each one of the three calibration windows, obtaining three different sets of K_n, K_f and θ_c functions (Section 4.2)
- The model calibrated according to the three calibration windows has been applied to predict forces for each one of the process operating window parameters combinations
- $RMSE_x$ has been selected as error index since $RMSE_z$ is negligible compared to $RMSE_x$ and $RMSE_y$ and $RMSE_y$ is highly correlated to $RMSE_x$
- $RMSE_x$ has been calculated for each one of the process operating window parameters combinations. Three different error maps have been obtained
- A regression model relating $RMSE_x$ to the process parameters has been carried out in the three cases in order to evaluate the most influencing factors on the prediction error. This analysis has led to some important considerations that give new information on the process mechanics and on the model capability to capture it:
    - All the parameters, apart from v_c, have a direct effect on the error, which means that the error increases when parameters values increase

- v_c is not significant on the error. This fact proves that the assumption according to which the model does not consider v_c as input parameter is correct
- a_p is significant on $RMSE_x$, but it is not significant on the relative error ($RMSE_x$ divided by the mean value of the peak F_x moduli along the five acquired periods). This fact points out that the error increases with a_p, but this could be a natural trend because also F_x increases with a_p.
- The $RMSE_x$ mean value calculated over the whole process operating window in the three different calibration window cases has pointed out as the "suggested" calibration window has a performance very close to the "complete" one even if based on 6 calibration tests against 72. The "reference" calibration window performance is the worst, even if it was applied in [37]. This fact proves that if the calibration tests are carefully selected, a good model prediction performance can be obtained also saving the employed resources. Also another important conclusion can be drawn, since this result proves that the mechanistic model object of this study and its cutting force coefficients are not independent from process parameters, but a different prediction performance can be obtained in function of the process parameters values used for the model calibration. Best calibration conditions seem to correspond to the highest process parameters values and, consequently, to the highest forces, conditions where the model prediction error is higher. Since the selected force model is representative for micromilling, the acquired knowledge is important and can be used to improve the model itself.

Figure 7 shows a comparisons between measured and predicted cutting forces for one tooth passage in case predicted forces very well agree with the measured ones (Figure 7(a)) and in case the model prediction performances is worse (Figure 7(b)) (i.e. where all the process

parameters are set at their highest values). The suggested calibration window has been applied in both the cases.

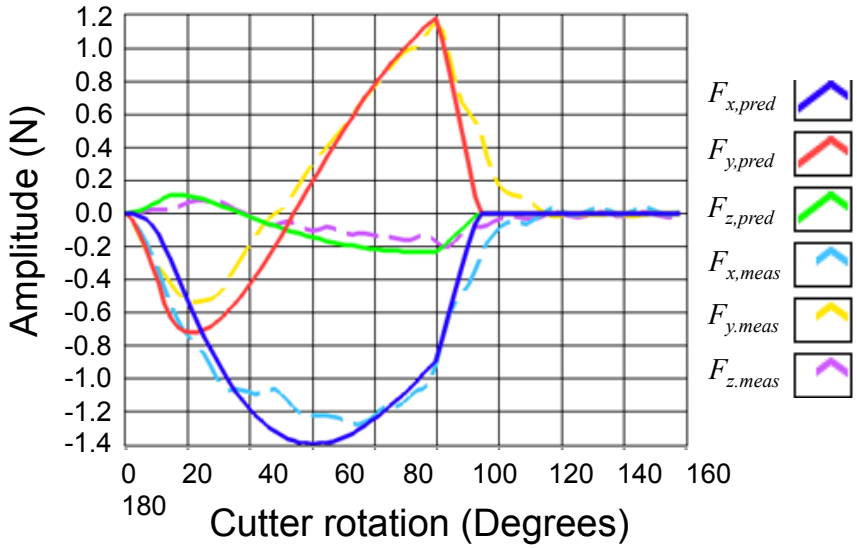

(a)

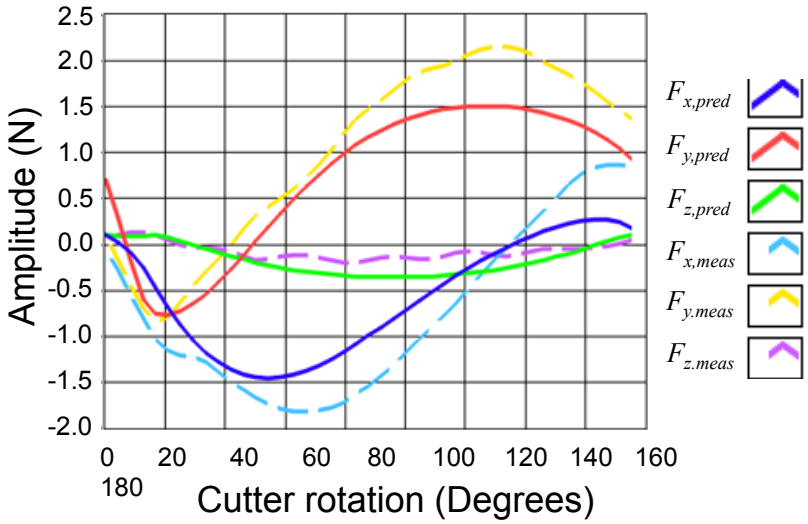

(b)

Figure 7: Comparison between measured and predicted cutting forces for one tooth passage. a) a_p = 0.1 mm; a_e = 0.250 mm (0.5D); f_z = 3 µm; v_c = 13.90 m/min. b) a_p = 0.1 mm; a_e = 0.5 mm (D); f_z = 4 µm; v_c = 28.04 m/min

9 Conclusions

The present study has been focused on the experimental calibration and validation of a highly representative mechanistic micromilling force prediction model. This relevant topic is rarely treated in the micromilling literature even if it determines the model performance and applicability.

It has been pointed out how the model prediction performance depends on an accurate calibration window selection, i.e. on a proper selection of the process parameters combinations to use for calibrating the model. The model and its cutting force coefficients can be consequently considered as dependent on the cutting conditions through the calibration experiments. The comparison among three different calibration windows has allowed to verify how calibrating the model in a region of the process operating window characterized by high cutting force values seems to be the best choice, as a confirmation of the relevance of forces on the overall process quality, including also the process predictability.

The model calibration can be carried out based on a small set of experiment if the calibration window position is correctly selected.

Reliable, accurate and repeatable calibration and validation tasks have required the application of objective definitions and accurate experimental procedures:

- The force acquisition experimental procedure has been carefully designed to take into account typical phenomena as the load cell bandwidth limitation, signal windowing and leakage and signal variability. Regarding this last point, the model has been improved, comparing to literature, to consider more force periods in the calibration phase, which makes it more statistically robust
- The model prediction error has been defined in order to allow comparisons. Other performance indexes could be introduced by further studies

- A clear and repeatable validation procedure based on the evaluation of the model prediction error over the whole process operating window has been introduced and applied.

The validation procedure has pointed out some fundamental considerations on the role of the cutting speed v_c and depth of cut a_p on the model prediction capability. The cutting speed has demonstrated to play a negligible role on the prediction error confirming the model hypothesis not to consider v_c among its input parameters. The depth of cut influences the force prediction error but, when the error is considered relatively to the force magnitude, the a_p effect disappears, as pointing out how the prediction error could increase at high a_p values simply because also forces are high in those conditions. Further studies could improve the model prediction capability by investigating the pointed out possibilities. These results demonstrate how new knowledge on the process mechanics could come from a rigorous calibration and validation procedure.

10 Acknowledgments

The authors are grateful to the "MI_crolab" staff, in particular Francesco Cacciatore and Massimo Goletti, for their invaluable support.

This study has been partly funded by Regione Lombardia, within the project "REMS: Rete Lombarda di Eccellenza per la Meccanica Strumentale e Laboratorio Esteso / Excellence Network for Instrumental Mechanics and Extended Laboratory" (Fondo per la promozione di Accordi istituzionali, d.reg. n°4779, 14/5/2009), and by the European Union Seventh Framework Programme FP7/2007-2013, under the grant agreement n° 285075 ("Innovative proactive Quality Control system for in-process multi-stage defect reduction" - MuProD).

11 References

[1] Ehmann KF, Kapoor SG, DeVor RE, Lazoglu I (1997) Machining process modeling: a review. J. Manuf. Sci. Eng. 119(4):655–663.

[2] van Luttervelt CA, Childs THC, Jawahir IS, Klocke F, Venuvinod PK, Altintas Y, Armarego EJA, Dornfeld D, Grabec I, Leopold J, Lindstrom B, Lucca D, Obikawa T, Shirakashi, Sato H (1998) Present situation and future trends in modeling of machining operations - Progress report of the CIRP working group 'modelling of machining operations'. CIRP Ann. 47(2):588–626.
[3] Liu X, DeVor RE, Kapoor SG, Ehmann KF (2004) The mechanics of machining at the microscale: assessment of the current state of the science. J. Manuf. Sci. Eng. 126: 666-678.
[4] Dornfeld D , Min S , Takeuchi Y (2006) Recent advances in mechanical micromachining. CIRP Ann-Manuf. Technol. 52:483-507.
[5] Dornfeld D, Lee DE (2007) Precision manufacturing. Springer.
[6] Arrazola PJ, Özel T, Umbrello D, Davies M, Jawahir IS (2013) Recent advances in modelling of metal machining processes. CIRP Ann-Manuf. Technol. 62:695-718.
[7] Weule H, Huntrup V, Tritschle H (2001) Micro-cutting of steel to meet new requirements in miniaturization. CIRP Ann-Manuf. Technol. 49:61-64.
[8] Liu X, DeVor RE, Kapoor SG (2006) An analytical model for the prediction of minimum chip thickness in micromachining. J. Manuf. Sci. Eng. 128:474–481.
[9] Subbiah S, Melkote SN (2007) Evidence of ductile tearing ahead of the cutting tool and modeling the energy consumed in material separation in micro-cutting. J. Manuf. Sci. Eng. 129:321-331.
[10] Wang J, Gong Y, Abba G, Antoine JF, Shi J (2009) Chip formation analysis in micromilling operation. Int. J. Adv. Manuf. Technol. 45:430–447.
[11] Jin X, Altintas Y (2012) Prediction of micro-milling forces with finite element method. J. Mater. Process. Technol. 212: 542–552
[12] Afazov SM, Ratchev SM, Segal J (2010) Modelling and simulation of micro-milling cutting forces. J. Mater. Process. Technol. 210:2154–2162.
[13] Komanduri R, Chandrasekaran N, Raff LM (1998) Effect of tool geometry in nanometric cutting: a molecular dynamics simulation approach. Wear. 219(1):84-97.
[14] Cai MB, Li XP, Rahman M (2007) Study of the mechanism of nanoscale ductile mode cutting of silicon using molecular dynamics simulation. Int. J. Mach. Tools Manuf. 47:75–80
[15] Kim CJ, Mayor JR, Ni J (2012) Molecular dynamics simulations of plastic material deformation in machining with a round cutting edge. Int. J. Precis. Eng. Manuf. 13(8):1303-1309.
[16] Budak E, Altintas Y, Armarego EJA (1996) Prediction of milling force coefficients from orthogonal cutting data. J. Manuf. Sci. Eng. 118:216-224.
[17] Lee P, Altintas Y (1996) 'Prediction of ball-end milling forces from orthogonal cutting data. Int. J. Mach. Tools Manuf. 36:1059–1072.
[18] Altintas Y, Lee P (1998) Mechanics and dynamics of ball end milling. J. Manuf. Sci. Eng. 120(4):684-692.
[19] Engin S, Altintas Y (2001) Mechanics and dynamics of general milling cutters - Part I: helical end mills. Int. J. Mach. Tools Manuf. 41(15):2195–2212.
[20] Bissacco G, Hansen HN, Slunsky J. (2008) Modelling the cutting edge radius size effect for force prediction in micro milling. CIRP Ann-Manuf. Technol. 57(1):113–116.
[21] Kaymakci M, Kilic ZM, Altintas Y (2012) Unified cutting force model for turning, boring, drilling and milling operations. Int. J. Mach. Tools Manuf. 54–55:34–45.
[22] Tuysuz O, Altintas Y, Feng HY (2013) Prediction of cutting forces in three and five-axis ball-end milling with tool indentation effect. Int. J. Mach. Tools Manuf. 66:66–81.
[23] Altintas Y, Kilic ZM (2013) Generalized dynamic model of metal cutting operations. CIRP Ann-Manuf. Technol. 62(1):47-50.

[24] Kumar M, Chang CJ, Melkote SN, Roshan Joseph V (2013) Modeling and analysis of forces in laser assisted micro milling. J. Manuf. Sci. Eng. 135 (4), 041018.
[25] Tlusty J, MacNeil P (1975) Dynamics of cutting forces in end milling. CIRP Ann. 24(1):21-25.
[26] Kline WA, DeVor RE, Lindberg JR (1982) The prediction of cutting forces in end milling with application of cornering cuts. Int. J. Mach. Tool Des. Res. 22(1):7–22.
[27] Sutherland JW, DeVor RE (1986) An improved method for cutting force and surface error prediction in flexible end milling systems. J. Eng. Ind.-Trans. ASME. 108(4):269–279.
[28] Bao WY, Tansel IN (2000) Modeling micro-end-milling operations - Part I: Analytical cutting force model. Int. J. Mach. Tools Manuf. 40(15):2155–2173.
[29] Bao WY, Tansel IN (2000) Modeling micro-end-milling operations - Part II: Tool run-out. Int. J. Mach. Tools Manuf. 40(15):2175-2192.
[30] Bao WY, Tansel IN (2000) Modeling micro-end-milling operations - Part III: Influence of tool wear. Int. J. Mach. Tools Manuf. 40(15):2193-2211.
[31] Zaman MT, Kumar AS, Rahman M, Sreeram S (2006) A three-dimensional analytical cutting force model for micro end milling operation. Int. J. Mach. Tools Manuf. 46(3-4):353–366.
[32] Malekian M, Park SS, Jun MBG (2009) Modeling of dynamic micro-milling cutting forces. Int. J. Mach. Tools Manuf. 49(7-8):586–598.
[33] Jun MBG, Goo C, Malekian M, Park SS (2012) A new mechanistic approach for micro end milling force modeling. J. Manuf. Sci. Eng. 134(1), 011006.
[34] Yucesan G, Xie Q, Bayoumi AE (1993) Determination of process parameters through a mechanistic force model of milling operations. Int. J. Mach. Tools Manuf. 33(4):627–641.
[35] Ko JH, Yun WS, Cho DW, Ehmann KF (2002) Development of a virtual machining system - Part1: Approximation of the size effect for cutting force prediction. Int. J. Mach. Tools Manuf. 42:1595–1605.
[36] Ko JH, Cho DW (2005) 3D ball-end milling force model using instantaneous cutting force coefficients. J. Manuf. Sci. Eng. 127:1–12.
[37] Lee HU, Cho DW, Ehmann KF (2008) A mechanistic model of cutting forces in micro-end-milling with cutting-condition-independent cutting forces coefficients. J. Manuf. Sci. Eng. 130(3), 031102.
[38] Vogler MP, Kapoor SG, DeVor RE (2004) On the modeling and analysis of machining performance in micro-endmilling - Part II: Cutting force prediction. J. Manuf. Sci. Eng. 126(4).695-705.
[39] Jun MBG, Liu X, DeVor RE, Kapoor SG (2006) Investigation of the dynamics of micro-end milling - Part 1: Model development. J. Manuf. Sci. Eng. 128(4):893–900.
[40] Jun MBG, Liu X, DeVor RE, Kapoor SG (2006) Investigation of the dynamics of micro-end milling - Part 2: Model validation and interpretation. J. Manuf. Sci. Eng. 128(4):901–912.
[41] Altintas Y, Jin X (2011) Mechanics of micro-milling with round edge tools. CIRP Ann-Manuf. Technol. 60:77–80.
[42] Waldorf DJ, DeVor RE, Kapoor SG (1998) Slip-line field for ploughing during orthogonal cutting, J. Manuf. Sci. Eng. 120:693-698.
[43] Jin X, Altintas Y (2011) Slip-line field model of micro-cutting process with round tool edge effect. J. Mater. Process. Technol. 211:339–355.
[44] Jin X, Altintas Y (2013) Chatter stability model of micro-milling with process damping. J. Manuf. Sci. Eng. 135 (3), 031011
[45] E. Korkmaz, B. Bediz, B. A. Gozen, O. B. Ozdoganlar (2014) Dynamic characterization of multi-axis dynamometers. Precision Engineering 38 148–161.
[46] Kistler© 9317B 3-Component Force Link Instruction Manual, http://www.kistler.com/us/en/product/force/9317B. Accessed 12-11-2013.

[47] Altintas Y, Park SS (2004) Dynamic compensation of spindle-integrated force sensors. CIRP Ann-Manuf. Technol. 53:305-308.
[48] Annoni M, Semeraro Q (2010) Factors affecting the force variability in micro-end-milling. 7th International Conference on Multi-Material Micro Manufacture (4M 2010), Bourg en Bresse and Oyonnax, France, 161-164.
[49] Kim CJ, Mayor JR, Ni J (2004) A static model of chip formation in microscale milling. J. Manuf. Sci. Eng. 126:710-718.
[50] Montgomery DC (2001) Design and analysis of experiments, 5th edition, Wiley, New York.